Nuclear Quantum Effects in Condensed Phase: The case of the "Association Band" of Liquid Water

Marco Cazzaniga,[1] Davide Moscato,[1, a)] Riccardo Conte,[1] and Michele Ceotto[1]
Dipartimento di Chimica, Università degli Studi di Milano, via Golgi 19, 20133 Milano, Italy

(*Electronic mail: michele.ceotto@unimi.it)

(*Electronic mail: marco.cazzaniga@guest.unimi.it)

(Dated: 9 February 2026)

The combination band just above 2000 cm^{-1} appearing in the IR spectrum of liquid water is well know from experiments and it is thought to be originated from the combination of bending motions of the water molecules and the large-amplitude libration modes of the condensed phase. While classical simulations cannot genuinely reproduce this band, here we show that this exquisitely quantum signal can be simulated by on-the-fly *ab initio* semiclassical molecular dynamics. The number of atoms involved in reproducing this combination band, which is also known as the "association band" of liquid water, shows that this condensed phase signal is quite local.

Keywords: Semiclassical, Condensed Phase, spectrum, water

I. INTRODUCTION

There is a combination band in the InfraRed (IR) absorption spectrum of liquid water that is so peculiar and well-known to deserve a moniker: The "association band". This name has been given after the features observed in this part of the spectrum in aqueous minerals, glasses or carbohydrate materials.[1] It is a weak and broad band centered at about 2130 cm^{-1}, and it has been assigned to the combination of the water monomer bendings with the libration motions.[2–4] Since librations are originally rotational normal modes which have been hindered by H-bonds between water molecules, the association band could unveil the intermolecular structure and dynamics of liquid water[5,6] and it represents a unique spectroscopic signal able to detect the morphology of the H-bonding network.

In previous simulations, this band has been not discussed in depth, given its low intensity compared with those of the stretching, bending and libration bands. However, despite its weak intensity, we believe that it is very important to focus on this signal to better understand the dynamical structure of liquid water, which can lead to new insights into chemical and biological processes. In fact, this band is present in all IR aqueous sample spectra and it represents a sort of local probe that can help one to decipher the complex H-bonding network and its collective ramification in addition to IR stretching signals and THz spectroscopy,[7], the relative strength of these bonds and the surrounding molecules role, where each water monomer is vibrating.

Only simulations that incorporate nuclear quantum effects can correctly reproduce combination bands that correspond to two vibrational quanta of excitations,[8] as well as reproduce other static and dynamical manifestations of quantum mechanics, such as the zero-point energy (ZPE) and tunneling. However, one may wonder if nuclear quantum mechanics is really needed for describing liquid water since quantum effects are sometimes manifest and sometimes are not. For example, some physical chemical properties of liquid water seem to display deviations from the classical behavior, while others are not.[9] Interestingly enough, a similar phenomenon is also observed in processes involving living organisms. More specifically, some prokaryotic organisms and bacteria tolerate a pure deuterated environment,[10] while 30% of deuteration is enough for killing healthy plants and mammals.[11–13] The reasons of this ambivalence reside on the fact that quantum effects are sometimes compensating each other. For instance, this is the case of ZPE, which enhances H-bonding with its stretching contributions and weakens it for its bending one. This is proven from the fact that going from the gas phase to the liquid one the symmetric stretching and bending frequencies are shifting from 3657 to 3404 cm^{-1} and from 1595 to 1644 cm^{-1}, respectively.[9] However, this is not the case of the association band signal because this nuclear quantum effect can be directly and unequivocally observed from the IR water spectrum. In this case, to correctly simulate it, one needs a nuclear quantum method able to potentially reproduce all vibrational levels and the corresponding transitions, including combinations, overtones and hot bands, in addition to the fundamental ones.

Apart from the trivial description of harmonic quanta of excitation, where combinations and overtones can be estimated by simply adding the integer multiples of the corresponding frequencies, there are essentially two main approaches for spectrum calculations: the time-independent and the time-dependent one. In the first case the full Hamiltonian is diagonalized and the spectrum is obtained by calculating the eigenvalues and the eigenfunctions of the nuclear problem. Vibrational perturbation theory (VPT2)[14] and vibrational configuration interaction (VCI)[15] are two accurate methods based on the time-independent approach.[16] In the second case, the Fourier transform is applied to the survival amplitude of a wavepacket to get the power spectrum, or to the dipole autocorrelation function to get the IR spectrum. Path integral molecular dynamics (PIMD) and related meth-

a)Currently at Department of Chemistry, Aarhus University, Langelandsgade 140, 8000 Aarhus C, Denmark

ods, such as RPMD, CMD, path-integral Liouville dynamics, quasi centroid molecular dynamics (QCMD), fast QCMD and Te PIGS[17–25] and semiclassical dynamics[26–31] are two accurate methods based on the time-dependent approach.

The simplest system that has been studied as a prototype of the association band is the one investigated by Rheinecker and Bowman, i.e. the Cl^- H_2O one,[32] where they observed a consistent intensity borrowing (and mechanical anharmonicity) in the combination band involving the bonded OH stretch and two quanta in the out-of-plane bend. A system closer to liquid water is given by the series of water cluster considered by McCoy,[33] where a variety of structural motifs were found to have intensity in the same frequency region of the liquid water association band. Actually, the same author[34] previously found spectroscopic features varying from 1939 to 2247 cm^{-1} in complexes of H_3O^+ with three argon atoms, nitrogen, methane, or water molecules. Interestingly, they found that the stronger the interaction between the H_3O^+ and the solvating molecules is, the more intense the association band spectroscopic features are. They concluded that the intensity of the liquid water association band, where the bending is anharmonically coupled to librations throughout the local water network interactions, is related to the strength of these interactions.

Moving up from these cluster prototypes and when it comes to complex systems such as the liquid water one, an additional problem is represented by the need of a full-dimensional potential energy surface (PES). In the case of a periodic-boundary-conditions simulation of liquid water, there are quite accurate, state of the art PESs available such as q-AQUA[35–37] and MB-POL.[38–40]

In the past, liquid water has been simulated both using PESs[26,41–44] and by means of on-the-fly molecular dynamics.[45,46] These simulations mainly focused on the accuracy in reproducing the main spectroscopic features of the IR spectrum of liquid water, which are the stretching, bending and libration bands. As far as the association band is concerned, linearized semiclassical calculations[47] mimic the presence of this band but they do not reproduce real-time coherences[48] and could not provide any specific physical insight. These simulations were focused on reproducing all the signals originated from all water molecules, without any specific distinction based on the molecular origin of each part of the bands.

Here, we aim at tracing back to the molecular level the origin of the association band signal by using semiclassically approximated quantum dynamics.[49–58] More specifically, we employ our divide-and-conquer semiclassical initial value representation approach (DC-SCIVR).[59] Within this framework the vibrational degrees of freedom (normal modes) are divided into subspaces. This procedure allows one to identify the most coupled modes and which portion of the spectrum is originated by each vibrational mode subspace. We apply this strategy to get physical insight into the association band obtained by simulating a box of liquid water by means of our on-the-fly *ab initio* semiclassical protocol.

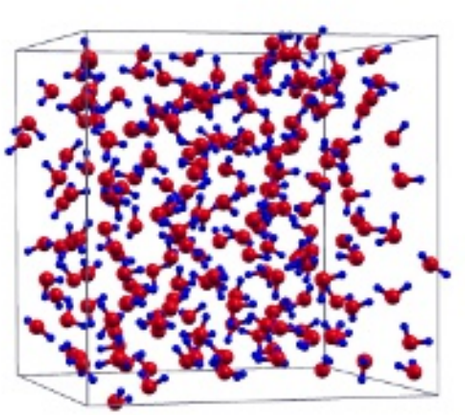

FIG. 1. Snapshot of the liquid water simulation cell: H atom in blu and O atom in dark red. Periodic boundary conditions are indicated by the cube edges.

II. COMPUTATIONAL METHODS

The simulation cell consists of a cubic box of 18 Å side containing 200 water molecules, and it is generated using the Packmol tool.[60] The obtained geometry is optimized via *ab initio* geometry relaxation and the dynamics simulation starts from a local minimum. A snapshot of the entire simulated system is reported in Fig. 1.

The *ab initio* calculations are performed with the Quantum-Espresso suite.[61,62] We adopt norm-conserving pseudopotentials obtained from the PseudoDojo website[63,64] with an energy cutoff of 85 Ry. Due to the dimension of the cell, the Brillouin zone is sampled using the Γ point only. We adopt a PBE parameterization for the Exchange and Correlation functional.[65] We validate our PBE approach against tests performed by adopting a revPBE[66] parametrization for the exchange potential V_{XC} and including Grimme dispersions (with zero damping and accounting for three body interactions),[67] as reported in the Supplementary Material (see Fig. S1).

Harmonic vibrational frequencies are computed by finite difference of the atomic forces in cartesian coordinates by adopting an atomic displacement of 0.01 Å, which allows to define the normal mode coordinates for the full periodic system and we will use this coordinate system for the rest of the simulations.

Quasi-Classical anharmonic vibrational frequencies are estimated by calculating the Time-Averaged velocity (momentum) autocorrelation function

$$I(E) = \frac{1}{2T} \sum_j \left| \int_0^T e^{iEt/\hbar} p_j(t) dt \right|^2 , \qquad (1)$$

where the summation over the j index runs over either normal modes or atomic velocities in Cartesian representation. Each

molecular dynamics trajectory is initialized at the equilibrium geometry and initial velocities correspond to the harmonic Zero Point Energy (ZPE) motion. This Born-Oppenheimer Molecular Dynamics (BOMD) is performed in the NVE ensemble and the atomic coordinates are evolved by means of a velocity Verlet algorithm for at least 2500 MD steps of 10 a.u. each, yielding 0.6 ps of dynamics in Cartesian coordinates. This classical approach allows us to estimate the contribution of fundamental transitions in the liquid water power spectrum. The Zero Point Energy leakage (ZPEL) will eventually cause the high-frequency modes to cool down and the low-frequency ones to heat up. Since an exact initial quantization of energy in the high-frequency modes is not achievable, we start from harmonic quantization, which overstimates the mode energy. The excess energy will flow into low-frequency modes during the dynamics, so to better deal with the ZPEL issue the latter are started with no energy if their harmonic frequency is below a given threshold. The low-frequency modes will gradually start to vibrate because of the ZPEL and contribute to the power spectrum. ZPEL is not an issue when using many (thousands) trajectories in semiclassical dynamics[68], however, a single semiclassical trajectory can not compensate the ZPEL effect.

To gain quantum insight, we employ semiclassical Molecular Dynamics, which adds quantum effects to simulations in the field of spectroscopy. Semiclassical methods are able to provide access to quantum power spectra by accounting quantum nuclear effects like ZPE, overtones and combination bands and relying only on classical BOMD trajectories.[8] The semiclassical approximation can be achieved by applying the Stationary Phase Approximation to the Feynman path integral.[69–73] Among the several possible formulations of the semiclassical propagator, we employ DC-SCIVR[59] to deal in an on-the-fly fashion with such a large dimensional system.[74–77] This approach allows one to reduce the system into subsystems where normal modes are collected according to their reciprocal couplings. To reduce the computational cost from running thousands of trajectories to a few ones or even a single trajectory, we also employ the Multiple Coherent states Semiclassical Initial Value Representation (MC-SCIVR) version of the semiclassical propagator for each DC-SCIVR vibrational subspace.[78–86] Within this method the power spectra $\mathrm{I}(E)$ can be obtained by the following sum over N_{traj} classical trajectories:

$$\mathrm{I}(E) = \frac{1}{N_{traj}} \sum_{j=1}^{N_{traj}} \frac{1}{2\pi\hbar T} \left| \int_0^T e^{i\left[S_t\left(\mathbf{p}_j(0),\mathbf{q}_j(0)\right)+Et+\phi_t\right]/\hbar} \langle \chi | \mathbf{p}_j(t), \mathbf{q}_j(t) \rangle dt \right|^2 \quad (2)$$

where T is the total trajectory simulation time, $S_t(\mathbf{p}(0),\mathbf{q}(0))$ is the classical action, ϕ_t is the phase of $C_t(\mathbf{p}(0),\mathbf{q}(0))$, which is the Herman-Kluk pre-exponential factor $C_t(\mathbf{p}(0),\mathbf{q}(0))$

$$C_t(\mathbf{p}(0),\mathbf{q}(0)) = \sqrt{\det\left|\frac{1}{2}\left(\mathbf{M_{qq}} + \Gamma^{-1}\mathbf{M_{pp}}\Gamma - i\hbar\Gamma\mathbf{M_{qp}} + \frac{i\Gamma^{-1}}{\hbar}\mathbf{M_{pq}}\right)\right|} \quad (3)$$

$C_t(\mathbf{p}(0),\mathbf{q}(0))$ is a complex number and ϕ_t=Phase$[C_t(\mathbf{p}(0),\mathbf{q}(0))]$ and where $M_{qq} = \partial \boldsymbol{q}(t)/\partial \boldsymbol{q}(0)$ etc., are the monodromy matrix elements. In Eq. (2) $|\mathbf{p}(t),\mathbf{q}(t)\rangle$ is a coherent state of the type[87–92]

$$\langle \mathbf{x}|\mathbf{p}(t),\mathbf{q}(t)\rangle = \left(\frac{\det(\Gamma)}{\pi^F}\right)^{1/4} \times e^{-(\mathbf{x}-\mathbf{q}(t))^T\Gamma(\mathbf{x}-\mathbf{q}(t))/2 + i\mathbf{p}^T(t)(\mathbf{x}-\mathbf{q}(t))/\hbar} \quad (4)$$

and in Eq.s (3) and (4) Γ is approximated to be a diagonal width matrix for bound state calculations, with coefficients usually numerically equal to the square root of the harmonic vibrational frequencies. The time evolution of $C_t(\mathbf{p}(0),\mathbf{q}(0))$ is computed through the solution of the equation of motion for the monodromy matrix M, for which the knowledge of the Hessian matrix along the MD trajectory is required. The way the MC-SCIVR method can contain the number of trajectories is by means of a suitable choice of the initial MD conditions. Also, a clever choice of the reference coherent states $|\chi\rangle$ can enhance the spectral features corresponding to the vibrational excitations under investigation avoiding the burden of the phase space integration required by other semiclassical molecular dynamics approaches. More specifically, the trajectory should be initialized with an energy close to a given quantum vibrational eigenvalue, which is approximated with its harmonic estimate, i.e. $\mathbf{p}_{\mathrm{eq}}^2/2m = \hbar\boldsymbol{\omega}(\mathbf{n}+1/2)$ and the corresponding reference superposition of coherent state is chosen as :

$$|\chi\rangle = |\mathbf{p}_{\mathrm{eq}},\mathbf{q}_{\mathrm{eq}}\rangle + \boldsymbol{\epsilon}\,|-\mathbf{p}_{\mathrm{eq}},\mathbf{q}_{\mathrm{eq}}\rangle \quad (5)$$

where $\boldsymbol{\epsilon}$ is a vector such that when all its elements are equal to 1, the ZPE peak and all even overtones intensities are enhanced, while when one of its component is equal to -1 the fundamental and the odd overtones of that mode component are enhanced.[81] Because of the large number of atoms present in our simulation cell, we limit our calculations to a single ZPE-trajectory and enhance the different spectroscopic features by using suitable combinations of coherent states for the reference state. Given the periodic motion of vibrations, even a short, tailored single trajectory is suitable to sample the relevant portion of the phase space, if the trajectory is long enough to include many periods of the vibrational motion.

Furthermore, the number of degrees of freedom is so huge that even the full dimensional Hessian matrix is out of reach. The full Hessian has been calculated in Cartesian coordinates only once for setting the normal mode coordinates. Each Hessian row/column along the chosen normal mode coordinate was calculated to find the DC-SCIVR vibrational subdivision. In this case, we calculate only the Hessian elements necessary for determining the vibrational subspace. For this reason, we employ a DC-SCIVR strategy[59,93–95] where the full

dimensional N_{vib} problem is reduced to a set of reduced dimensional ($M < N_{vib}$) ones. Specifically, the power spectrum $\mathrm{I}(E)$ of Eq. (2) is further approximated as the convolution of partial spectra $\widetilde{\mathrm{I}}(E)$ computed in M-dimensional subspaces of the full N_{vib}-dimensional space. Thus, the DC-SCIVR power spectrum formula is

$$\widetilde{\mathrm{I}}(E) = \frac{1}{2\pi\hbar T} \left| \int_0^T e^{i\left[\tilde{S}_t(\tilde{\mathbf{p}}(0),\tilde{\mathbf{q}}(0))+Et+\tilde{\phi}_t\right]/\hbar} \langle \tilde{\boldsymbol{\chi}} | \tilde{\mathbf{p}}(t), \tilde{\mathbf{q}}(t) \rangle dt \right|^2 \quad (6)$$

where all the quantities with the tilde superscript are evaluated by projecting the full dimensional ones onto the M-subspace. In this way we can drastically reduce the dimensionality of the semiclassical calculation. For most of the quantities in Eq. (6) the projection onto each subspace starting from the full dimensional one consists in taking the related vector components, except for the classical action $\tilde{S}_t$, due to the non-separability of the potential energy term. We get rid of this issue by assuming the following expression for the reduced dimensional potential

$$\tilde{V}_S(\tilde{\mathbf{q}}_M(t)) = V\left(\tilde{\mathbf{q}}_M(t); \mathbf{q}_{N_{vib}-M}(t)\right) - V\left(\mathbf{q}_M^{eq}; \mathbf{q}_{N_{vib}-M}(t)\right) \quad (7)$$

where $\boldsymbol{q}_M^{eq}$ are the starting values of the positions for the degrees of freedom that belong to the M-dimensional subspace S. The subspace subdivision should pair the strongly coupled modes in the same subspace. Among the different approaches developed in our group,[93,96] in the present work we employ an adapted version of the "Hessian" method[69,93] for the vibrational space subdivision. This consists in primarily choosing a mode of interest and then find the ones most coupled to it to build up the spectroscopic signal related to that mode. In our case we focus on the association band and we choose bending modes that can be associated to the bending motion of a single molecule in the liquid. In the present version of the "Hessian" method, the amount of coupling with other normal modes is estimated through the average of the modulus of the Hessian line/row row/column corresponding to the addressed bending $\partial^2 V/\partial q_{Mode}\partial q_i$ along the MD trajectory. The Hessian elements are calculated by finite differences of the atomic forces in normal mode coordinates, in order to avoid the calculation of the entire matrix in a similar way as in Ref. 97. The finite difference displacement was $5\times10^{-4}/\omega_i$ where ω_i is the harmonic frequency of the mode. Then, the off-diagonal elements ($i \neq Mode$) sorted in descending order provide the order in which the modes enters in the subspace. We limit the subspace up to the first coupled libration, whose combination is contributing to the association band signal together with other possible normal modes. To reduce the computational cost, we calculate only the Hessian elements of the sub-blocks which correspond to the vibrational subspace of the chosen bending mode. We also optimize the number of partial Hessian estimates, by employing a trajectory procedure based on the neural gas algorithm.[98] By employing 100 neurons we found an optimal compromise between accuracy and computational overheads.

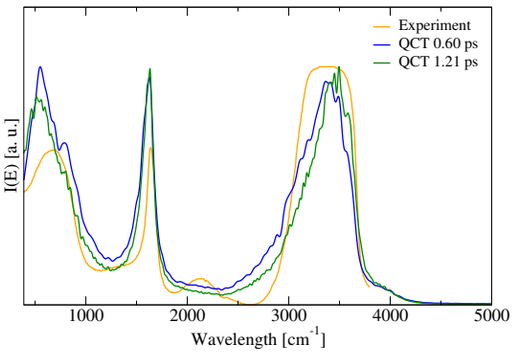

FIG. 2. QCT VDOS (computed using the correlator in terms of atomic velocities) in Cartesian coordinates for two different durations of the MD simulation. The experimental IR spectrum of liquid water is reported in orange.

III. RESULTS AND DISCUSSION

Quasi-classical trajectory (QCT) results obtained using Eq. (1) are reported in Fig. 2 and compared with the experimental IR spectrum of liquid water.[99] Our planewave PBE *ab initio* level of theory is clearly accurate enough to reproduce the main spectroscopic features. The simulated libration, bending and stretching bands reproduce quite faithfully the corresponding experimental frequency band intervals. We do not consider a direct comparison in terms of intensity since we are simulating the vibrational density of states (VDOS) and the experiment reports the IR absorption spectrum. We make this choice because we are focusing on a single bending+libration signal and to the atomistic picture explanation behind the association band. We can observe only a small deviation between the simulation and the experimental spectra at the lowest frequencies. We attribute this deviation to two main reasons. The first one is that the Cartesian coordinate simulation does include all modes of vibration, also the lower frequency ones. The other is that the zero point energy leakage is enhancing the lower frequency mode intensities. Apart from this, the main discrepancy between the classical VDOS and the experimental IR signal is in the association band region. The classical calculation can not reproduce the association band around 2100 cm^{-1}. To exclude any numerical issue, we have tested different computational setups, including longer trajectories with more statistics, and the same VDOS calculations in normal mode coordinates is found (see Fig. S2). The conclusion is always the same regardless the computational setup, i.e. in a classical simulation the association band is missing.

One may wonder if the association band is somehow hidden below the baseline of the QCT spectra reported in Fig. 2. To clarify this point, we report in Fig. 3 the signal originated from two specific modes that we have identified between possible candidates for generating the association band. As a reference, the harmonic frequency estimate of these modes are reported in Fig. 3 as vertical arrows. Both spectra do not significantly contribute to the VDOS portion of the spectrum above

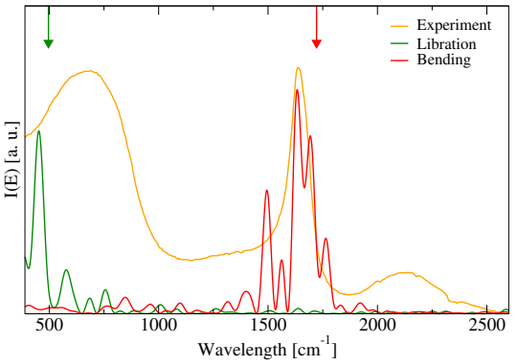

FIG. 3. Selected QCT VDOS of a bending (red line) and a libration (green line) modes. The vertical arrows indicate the harmonic estimate of the two modes. Experimental IR absorption spectrum is in orange.

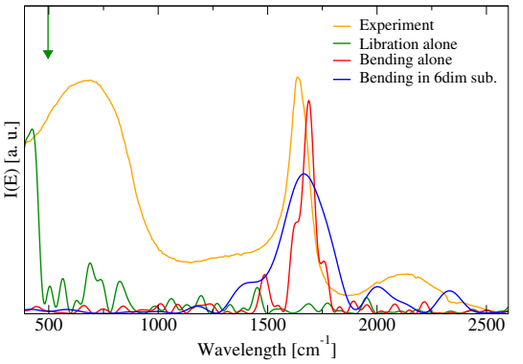

FIG. 4. DC-SCIVR power spectra calculations. Green and red lines are from the monodimensional vibrational subspaces of the libration and bending modes of Fig. 3. The blue line is for the same bending mode but in a six-dimensional vibrational subspace. ZPE has been shifted to zero.

2000 cm^{-1}. However, both libration and bending signal are composed of several splittings and side bands because of the strong coupling between these modes and many others present in liquid water. This shows that normal modes in liquid water are quite complex and different from those of gas phase water.

We now turn to our quantum dynamics VDOS calculations in semiclassical approximation and consider the VDOS signal originated by the same modes as in Fig. 3. Recalling that our DC-SCIVR approach allows us to divide the entire vibrational space into arbitrary dimensional subspaces up to monodimensional ones, and thanks to our divide-and-conquer approach,[59,98] we get of the Hessian matrices in the subspace at each time-step and calculate the monodromy matrix evolution. We recall here that in our DC-SCIVR approach, the classical mode dynamics is fully coupled even if modes belong to different vibrational subspaces, since the original classical trajectory is a full dimensional one. It is the semiclassical treatment that is factorized into subspaces and this includes mainly the approximation of the pre-exponential factor and the classical action, as reported in Eq. 6.

If we force the same bending and libration modes described above to belong to monodimensional vibrational subspaces and calculate the VDOS semiclassical signal, we obtain the green and red spectra reported in Fig. 4 for the libration and bending motion, respectively. The green and red arrows in Fig. 4 indicate the harmonic estimates as a reference and as already reported in Fig. 3. We stress that we employ in our DC-SCIVR calculations the same classical trajectory used for the QCT calculation. The libration and bending signals are quite similar to the corresponding classical ones of Fig. 3, with the exception that quantum effects within the same monodimensional subspace are accounted for. In our case, the possible quantum effects are the presence of overtone peaks, and this can be seen for the libration (green) line of Fig. 4 if compared with the QCT parent one of Fig. 3. Small intensity overtones or combination peaks can be observed also in the bending signal, especially in the region above 2000 cm^{-1}. When we improve the semiclassical approximation by allowing for the bending motion to be semiclassically coupled to other modes in a six-dimensional vibrational subspace, we obtain the signal reported in blue in Fig. 4. This association band signal contribution is compatible but different from a previous Multimode Embedded Local Monomer calculation,[100][Rossi et al., J. Chem. Phys. 141, 181101 (2014)] mainly because in that case all combination bands are considered, while here we are focusing on a single bending+libration contribution.

This vibrational subspace includes mainly stretching modes, as well as bending ones, as reported in Table S1 of the Supporting Material file. In Table S1 the modes are sorted in decreasing coupling order with respect to the bending one, and the six-dimensional vibrational subspace is delimited by the horizontal line. The coupling has been estimated from the row/column Hessian matrix averaged over the trajectory and using our divide-and-conquer procedure described above. This VDOS clearly shows a significant contribution in the association band frequency region and our DC-SCIVR calculation indicates that it is the cooperation between the bending mode and all these other modes belonging to the same vibrational subspace to originate the association band. The libration mode is not the sole actor that shapes the association band. Indeed, we find that there are some stretching modes, i.e. with frequency higher than 3100 cm^{-1}, which are strongly coupled to the bending one, according to our algorithm. Even if minor compared to direct coupling effects,[1][J. Phys. Chem. B 2018, 122, 9, 2587-2599] these modes indirectly contribute by coupling with the bending to the shape and intensity of the association band.

Fig. 5 reports the VDOS signal originated from one of the stretching mode belonging to the aforementioned six-dimensional vibrational subspace. Even if the main VDOS of this mode lies, as expected, in the stretching band, a non-negligible contribution is present in the combination band region. We consider the signal originated by this mode both when semiclassically forced in a monodimensional subspace and when fully coupled to the bending one in the six-dimensional subspace. The amount of VDOS is increasing when allowing the modes to be semiclassicaly coupled on the top of the already classical trajectory coupling. Ultimately, the

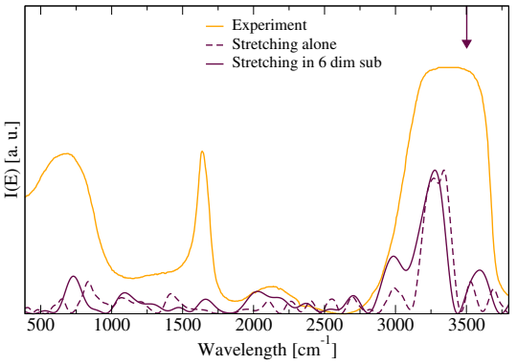

FIG. 5. DC-SCIVR power spectra calculations. Maroon dashed line is for the monodimensional vibrational subspace of a stretching mode chosen inside the subspace. Maroon solid line is for the same stretching mode but in a six-dimensional vibrational subspace. ZPE has been shifted to zero.

association band signal is originated by the coupling between several modes, as those reported in Table S1. Specifically, the role of such coupled modes, like the stretching ones which are far from the frequency range of the association band, is to include the contribution of other librational modes. These modes are not directly or strongly coupled to the target bending but coupled to the stretches and contribute indirectly to the signal of the association band. Thus, it clear that the VDOS contribution to the association bands is originated also from librational modes, which are not directly coupled to the bending.

To gain further physical insights, we visualize the pair of bending and libration normal modes that are responsible for contributions to the association band. Fig. 6 shows the nuclear displacements corresponding to the normal mode vectors of the bending and its coupled libration, as an example, while Fig. S3 in the Supplementary Material file shows the displacements of all the modes belonging to the same subspace. The direction and the length of the arrows of Fig. 6 reproduce the nuclear displacements and the periodic simulating box boundaries are indicated by continuous black lines. In Section II of the Supplementary Material file, we report the same type of representation for some stretching modes belonging to the same vibrational subspace of the bending one. We also consider other bending mode subspaces and the related libration and stretching coupled modes. We report these bending and libration modes in the SI (Section S-III). and we observe that even if the bending ones can not be attributed to a single water molecule, the libration modes are quite local. The main feature that we can infer from the observation of Fig. 6 and the other ones in the Supplementary Material file is that the associate libration and stretching modes are quite local, i.e. the involved atoms are mainly those of the same water molecules and of the nearest neighbor ones. In some cases we can observe more than few water molecules cooperating for the libration signal, however these kinds of motion are definitely more local than typical phonon modes.

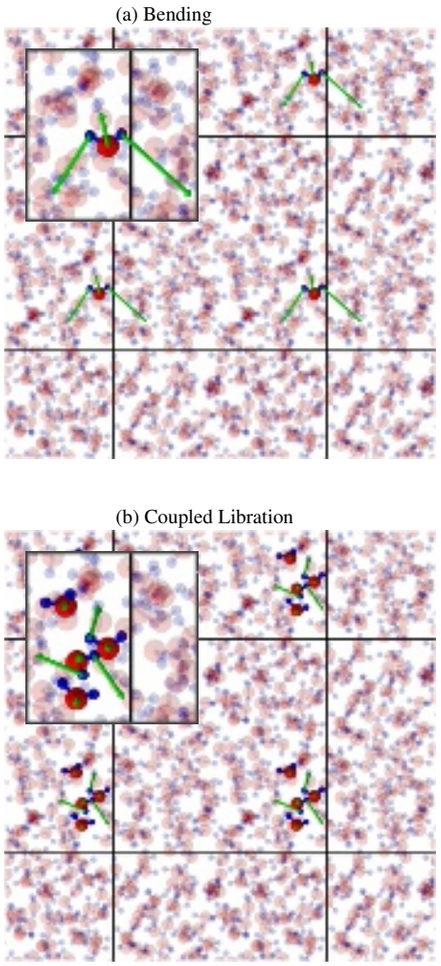

FIG. 6. Harmonic eigen-displacement of a bending mode and the first coupled libration one. The plot reports the eigen-displacement only of those atoms whose modulus is larger than half the maximum for H or O atoms. The length of the arrows corresponds to 7 times the modulus for H atoms and 35 times for O atoms.

IV. CONCLUSIONS

In this paper we exploit a quantum dynamics tool, the DC-SCIVR method, to shed light on the liquid water nuclear vibrational association band. Specifically, we focus on understanding which kind of modes are responsible for this spectroscopic signal. Indeed, we find that it is not just purely a matter of libration+bending coupling and that other modes are involved, most of them of the stretching type. These modes are strongly coupled to the bending one and they need to be included in the vibrational subspace of the bending mode in order to obtain a proper spectroscopic signal in the association band region. Actually, these modes cooperate for generating the signal in the association band region. In few words, even if their frequencies and eigen-displacements clearly suggest the stretching contribution, in a multidimensional quan-

tum picture their contribution to the total VDOS includes also the association band signal through their coupling to additional librational modes not included in the working subspace. These results confirm that the association band is a genuine H-bonding network signal which includes all types of modes, and that the topology of the involved H-bonding is quite variegated. This includes all kinds of atomic displacements and it cannot be associated with a few atomic displacements even in a first order harmonic approximation. Instead, there are many atoms involved in the association band signal. However, we could not find any example of a fully delocalized H-bonding, as it is the case in periodic solid systems as ice, for example. This is a clear factor which distinguishes the liquid phase from the solid one.

ACKNOWLEDGMENTS

The authors are deeply grateful to Jianshu Cao for his inspiring contributions to condensed phase quantum dynamics. We acknowledge the CINECA award under the ISCRA initiative, for the availability of high performance computing resources and support (projects CombH2O and SemDynHP).

SUPPLEMENTARY MATERIAL

See supplementary material for additional graphics and tables. Specifically we report a power spectrum comparison between different DFT functionals, between different system of reference (Cartesian vs normal mode), a table with the normal mode of the bending and the related association band vibrational subspace, and several eigen-displacements plots.

DATA AVAILABILITY STATEMENT

The data that support the findings of this study are available from the corresponding author upon reasonable request.

[1] P. K. Verma, A. Kundu, M. S. Puretz, C. Dhoonmoon, O. S. Chegwidden, C. H. Londergan, and M. Cho, J. Phys. Chem. B **122**, 2587–2599 (2018), pMID: 29095618, https://doi.org/10.1021/acs.jpcb.7b09641.
[2] J. J. Fox and A. Martin, Proc. R. Soc. Lond. A Math. Phys. Sci. **174**, 234 (1940).
[3] J. E. Bertie, M. K. Ahmed, and H. H. Eysel, J. Phys. Chem. **93**, 2210 (1989).
[4] J. E. Bertie and Z. Lan, Appl. Spectrosc. **50**, 1047 (1996).
[5] H. A. Al-Abadleh and V. Grassian, Langmuir **19**, 341 (2003).
[6] S. Giuffrida, G. Cottone, and L. Cordone, Phys. Chem. Chem. Phys. **19**, 4251 (2017).
[7] C. Lanzi, D. Mani, H. Ashraf, R. Conte, G. Schwaab, M. Havenith, and M. Ceotto, J. Phys. Chem. Lett. **17**, 888 (2026).
[8] J.-X. Zeng, R. Conte, and M. Ceotto, J. Chem. Phys. **163**, 194114 (2025).
[9] M. Ceriotti, W. Fang, P. G. Kusalik, R. H. McKenzie, A. Michaelides, M. A. Morales, and T. E. Markland, Chem. Rev. **116**, 7529 (2016).
[10] O. V. Mosin, V. I. Shvets, D. A. Skladnev, and I. Ignatov, Russ. J. Biopharm. **4**, 11 (2012).
[11] D. M. Czajka, A. J. Finkel, C. S. Fischer, and J. J. Katz, Am. J. Physiology-Legacy Cont. **201**, 357 (1961).
[12] J. F. Thomson, Ann. N. Y. Acad. Sci. **84**, 736 (1960).
[13] D. Kushner, A. Baker, and T. Dunstall, Can. J. Physiol. Pharmacol. **77**, 79 (1999).
[14] V. Barone, M. Biczysko, J. Bloino, M. Borkowska-Panek, I. Carnimeo, and P. Panek, Int. J. Quantum Chem. **112**, 2185 (2011).
[15] J. M. Bowman, S. Carter, and X. Huang, Int. Rev. Phys. Chem. **22**, 533 (2003).
[16] O. Christiansen, J. Chem. Phys. **120**, 2149–2159 (2004).
[17] S. Habershon, D. E. Manolopoulos, T. E. Markland, and T. F. Miller III, Annu. Rev. Phys. Chem. **64**, 387 (2013).
[18] I. R. Craig and D. E. Manolopoulos, J. Chem. Phys. **121**, 3368 (2004).
[19] J. Cao and G. A. Voth, J. Chem. Phys. **100**, 5093 (1994).
[20] J. Cao and G. A. Voth, J. Chem. Phys. **100**, 5106 (1994).
[21] T. Begušić and G. A. Blake, Nat. Commun. **14**, 1950 (2023).
[22] J. Liu and Z. Zhang, J. Chem. Phys. **144** (2016).
[23] J. E. Lawrence, A. Z. Lieberherr, T. Fletcher, and D. E. Manolopoulos, J. Phys. Chem. B **127**, 9172 (2023).
[24] G. Trenins, M. J. Willatt, and S. C. Althorpe, J. Chem. Phys. **151** (2019).
[25] M. Ceriotti and D. E. Manolopoulos, Phys. Rev. Lett. **109**, 100604 (2012).
[26] J. Liu and W. H. Miller, J. Chem. Phys. **127**, 114506 (2007).
[27] X. Sun, H. Wang, and W. H. Miller, J. Chem. Phys. **109**, 7064 (1998).
[28] A. L. Kaledin and W. H. Miller, J. Chem. Phys. **118**, 7174 (2003).
[29] C. Lanzi, C. Aieta, M. Ceotto, and R. Conte, J. Chem. Phys. **160**, 214107 (2024).
[30] C. Lanzi, C. Aieta, M. Ceotto, and R. Conte, J. Chem. Phys. **163** (2025).
[31] C. Aieta, M. Cazzaniga, D. Moscato, C. Lanzi, L. Bocchi, M. M. Costanza, M. Ceotto, and R. Conte, Rend. Lincei Sci. Fis. Nat. , 1 (2025).
[32] J. Rheinecker and J. M. Bowman, J. Chem. Phys. **125** (2006).
[33] A. B. McCoy, J. Phys. Chem. B **118**, 8286 (2014).
[34] A. B. McCoy, T. L. Guasco, C. M. Leavitt, S. G. Olesen, and M. A. Johnson, Phys. Chem. Chem. Phys. **14**, 7205 (2012).
[35] Q. Yu, C. Qu, P. L. Houston, R. Conte, A. Nandi, and J. M. Bowman, J. Phys. Chem. Letts. **13**, 5068 (2022).
[36] C. Qu, Q. Yu, P. L. Houston, R. Conte, A. Nandi, and J. M. Bowman, J. Chem. Theory Comput. **19**, 3446 (2023).
[37] Q. Yu, J. M. Bowman, C. Qu, A. Nandi, R. Conte, and P. L. Houston, Mol. Phys. , e2536184 (2025).
[38] G. R. Medders, V. Babin, and F. Paesani, J. Chem. Theory Comput. **10**, 2906 (2014).
[39] M. Riera, C. Knight, E. F. Bull-Vulpe, X. Zhu, H. Agnew, D. G. A. Smith, A. C. Simmonett, and F. Paesani, J. Chem. Phys. **159** (2023), 10.1063/5.0156036.
[40] S. Gupta, E. F. Bull-Vulpe, H. Agnew, S. Iyer, X. Zhu, R. Zhou, C. Knight, and F. Paesani, J. Chem. Theory Comput. **21**, 1838–1849 (2025).
[41] S. Habershon, G. S. Fanourgakis, and D. E. Manolopoulos, J. Chem. Phys. **129**, 074501 (2008).
[42] F. Paesani, Acc. Chem. Res. **49**, 1844 (2016).
[43] F. Paesani, S. S. Xantheas, and G. A. Voth, J. Phys. Chem. B **113**, 13118 (2009).
[44] D. Ojha, A. Henao, and T. D. Kühne, J. Chem. Phys. **148** (2018).
[45] O. Marsalek and T. E. Markland, J. Phys. Chem. Lett. **8**, 1545 (2017).
[46] A. P. Gaiduk, J. Gustafson, F. Gygi, and G. Galli, J. Phys. Chem. Lett. **9**, 3068 (2018).
[47] X. Liu and J. Liu, Mol. Phys. **116**, 755 (2018).
[48] T. Plé, S. Huppert, F. Finocchi, P. Depondt, and S. Bonella, J. Chem. Phys. **155** (2021).
[49] W. H. Miller, J. Phys. Chem. A **105**, 2942 (2001).
[50] F. Grossmann, J. Chem. Phys. **103**, 3696 (1995).
[51] E. Pollak, "The Semiclassical Initial Value Series Representation of the Quantum Propagator," in *Quantum Dynamics of Complex Molecular Systems* (Springer Berlin Heidelberg, Berlin, Heidelberg, 2007) pp. 259–271.
[52] R. Conte and E. Pollak, J. Chem. Phys. **136**, 094101 (2012).
[53] M. S. Church, S. V. Antipov, and N. Ananth, J. Chem. Phys. **146**, 234104 (2017).
[54] M. Church, S. V. Antipov, and N. Ananth, J. Chem. Phys. **146**, 234104 (2017).
[55] B. Gu and S. Garashchuk, J. Phys. Chem. A **120**, 3023 (2016).
[56] T. Begušić and J. Vaníček, J. Chem. Phys. **153**, 024105 (2020).
[57] T. Begušić and J. Vaníček, J. Chem. Phys. **153**, 184110 (2020).
[58] L. Bonnet, Chem. Phys. Lett. **851**, 141459 (2024).

[59]M. Ceotto, G. Di Liberto, and R. Conte, Phys. Rev. Lett. **119**, 010401 (2017).
[60]L. Martínez, R. Andrade, E. G. Birgin, and J. M. Martínez, J. Comput. Chem. **30**, 2157 (2009).
[61]P. Giannozzi, S. Baroni, N. Bonini, M. Calandra, R. Car, C. Cavazzoni, D. Ceresoli, G. L. Chiarotti, M. Cococcioni, I. Dabo, *et al.*, J. Phys.: Cond. matt. **21**, 395502 (2009).
[62]P. Giannozzi, O. Baseggio, P. Bonfà, D. Brunato, R. Car, I. Carnimeo, C. Cavazzoni, S. De Gironcoli, P. Delugas, F. Ferrari Ruffino, *et al.*, J. Chem. Phys. **152** (2020).
[63]M. van Setten, M. Giantomassi, E. Bousquet, M. Verstraete, D. Hamann, X. Gonze, and G.-M. Rignanese, Comput. Phys. Commun. **226**, 39 (2018).
[64]`http://www.pseudo-dojo.org/`.
[65]J. P. Perdew, K. Burke, and M. Ernzerhof, Phys. Rev. Lett. **77**, 3865 (1996).
[66]Y. Zhang and W. Yang, Phys. Rev. Lett. **80**, 890 (1998).
[67]S. Grimme, J. Antony, S. Ehrlich, and H. Krieg, J. Chem. Phys. **132**, 154104 (2010).
[68]M. Buchholz, E. Fallacara, F. Gottwald, M. Ceotto, F. Grossmann, and S. D. Ivanov, Chem. Phys. **515**, 231 (2018).
[69]R. Conte and M. Ceotto, Quantum Chemistry and Dynamics of Excited States: Methods and Applications , 595 (2020).
[70]R. Conte, G. Mandelli, G. Botti, D. Moscato, C. Lanzi, M. Cazzaniga, C. Aieta, and M. Ceotto, Chem. Sci. **16**, 20 (2025).
[71]R. Conte, C. Aieta, M. Cazzaniga, and M. Ceotto, J. Phys. Chem. Lett. **15**, 7566 (2024).
[72]J.-X. Zeng, S. Yang, Y.-C. Zhu, W. Fang, L. Jiang, E.-G. Wang, D. H. Zhang, and X.-Z. Li, J. Phys. Chem. A **127**, 2902 (2023).
[73]J.-X. Zeng and X.-Z. Li, Comput. Mater. Today **6**, 100032 (2025).
[74]E. Fallacara, F. Finocchi, M. Cazzaniga, S. Chenot, S. Stankic, and M. Ceotto, Angw. Chemie Intl. Ed. **63**, e202409523 (2024).
[75]D. Moscato, G. Mandelli, M. Bondanza, F. Lipparini, R. Conte, B. Mennucci, and M. Ceotto, J. Am. Chem. Soc. **146**, 8179 (2024).
[76]D. Moscato, F. Gabas, R. Conte, and M. Ceotto, J. Biomol. Struct. Dyn. (2023), 10.1080/07391102.2023.2180435.
[77]M. Cazzaniga, M. Micciarelli, F. Gabas, F. Finocchi, and M. Ceotto, J. Phys. Chem. C **126**, 12060 (2022).
[78]M. Ceotto, S. Atahan, S. Shim, G. F. Tantardini, and A. Aspuru-Guzik, Phys. Chem. Chem. Phys. **11**, 3861 (2009).
[79]M. Ceotto, S. Atahan, G. F. Tantardini, and A. Aspuru-Guzik, J. Chem. Phys. **130**, 234113 (2009).
[80]M. Ceotto, D. Dell' Angelo, and G. F. Tantardini, J. Chem. Phys. **133**, 054701 (2010).
[81]M. Ceotto, G. F. Tantardini, and A. Aspuru-Guzik, J. Chem. Phys. **135**, 214108 (2011).
[82]M. Ceotto, S. Valleau, G. F. Tantardini, and A. Aspuru-Guzik, J. Chem. Phys. **134**, 234103 (2011).
[83]R. Conte, A. Aspuru-Guzik, and M. Ceotto, J. Phys. Chem. Lett. **4**, 3407 (2013).
[84]G. Bertaina, G. Di Liberto, and M. Ceotto, J. Chem. Phys. **151**, 114307 (2019).
[85]F. Gabas, R. Conte, and M. Ceotto, J. Chem. Theory Comput. **16**, 3476 (2020).
[86]F. Gabas, G. Di Liberto, and M. Ceotto, J. Chem. Phys. **150**, 224107 (2019).
[87]E. J. Heller, Acc. Chem. Res. **14**, 368 (1981).
[88]E. J. Heller, J. Chem. Phys. **75**, 2923 (1981).
[89]E. J. Heller, J. Chem. Phys. **94**, 2723 (1991).
[90]D. V. Shalashilin and M. S. Child, J. Chem. Phys. **115**, 5367 (2001).
[91]M. F. Herman and E. Kluk, Chem. Phys. **91**, 27 (1984).
[92]E. Kluk, M. F. Herman, and H. L. Davis, J. Chem. Phys. **84**, 326 (1986).
[93]G. Di Liberto, R. Conte, and M. Ceotto, J. Chem. Phys. **148**, 014307 (2018).
[94]G. Di Liberto, R. Conte, and M. Ceotto, J. Chem. Phys. **148**, 104302 (2018).
[95]R. Conte, F. Gabas, G. Botti, Y. Zhuang, and M. Ceotto, J. Chem. Phys. **150** (2019), 10.1063/1.5109086.
[96]M. Gandolfi, A. Rognoni, C. Aieta, R. Conte, and M. Ceotto, J. Chem. Phys. **153**, 204104 (2020).
[97]M. Cazzaniga, M. Micciarelli, F. Moriggi, A. Mahmoud, F. Gabas, and M. Ceotto, J. Chem. Phys. **152**, 104104 (2020).
[98]M. Gandolfi and M. Ceotto, J. Chem. Theory Comput. **17**, 6733 (2021).
[99]Coblentz Society, Inc., "Evaluated Infrared Reference Spectra" in NIST Chemistry WebBook, **NIST Standard Reference Database Number 69**, Eds. P.J. Linstrom and W.G. Mallard, National Institute of Standards and Technology, Gaithersburg MD, 20899, https://doi.org/10.18434/T4D303.
[100]M. Rossi, H. Liu, F. Paesani, J. Bowman, and M. Ceriotti, J. Chem. Phys. **141**, 181101 (2014).